Bulletin of the Seismological Society of America, Vol. 88, No. 5, pp. 1182–1197, October 1998

Modeling Dynamic Rupture in a 3D Earthquake Fault Model

by R. Madariaga, K. Olsen, and R. Archuleta

Abstract We propose a fourth-order staggered-grid finite-difference method to study dynamic faulting in three dimensions. The method uses an implementation of the boundary conditions on the fault that allows the use of general friction models including slip weakening and rate dependence. Because the staggered-grid method defines stresses and particle velocities at different grid points, we preserve symmetry by implementing a two-grid-row "thick" fault zone. Slip is computed between points located at the borders of the fault zone, while the two components of shear traction on the fault are forced to be symmetric inside the fault zone. We study the properties of the numerical method comparing our simulations with well-known properties of seismic ruptures in 3D. Among the properties that are well modeled by our method are full elastic-wave interactions, frictional instability, rupture initiation from a finite initial patch, spontaneous rupture growth at subsonic and supersonic speeds, as well as healing by either stopping phases or rate-dependent friction. We use this method for simulating spontaneous rupture propagation along an arbitrarily loaded planar fault starting from a localized asperity on circular and rectangular faults. The shape of the rupture front is close to elliptical and is systematically elongated in the in-plane direction of traction drop. This elongation is due to the presence of a strong shear stress peak that moves ahead of the rupture in the in-plane direction. At high initial stresses the rupture front becomes unstable and jumps to super-shear speeds in the direction of in-plane shear. Another interesting effect is the development of relatively narrow rupture fronts due to the presence of rate-weakening friction. The solutions for the "thick fault" boundary conditions scale with the slip-weakening distance (D_0) and are stable and reproducible for D_0 greater than about 4 in terms of $2T_u/\mu \times \Delta x$. Finally, a comparison of scalar and vector boundary conditions for the friction shows that slip is dominant along the direction of the prestress, with the largest deviations in slip-rate direction occurring near the rupture front and the edges of the fault.

Introduction

Earthquake source dynamics provides key elements for the prediction of strong ground motion and to understand the physics of earthquake initiation, propagation, and healing (see, e.g., Kostrov and Das, 1989; Scholz, 1989). Recent studies of rupture processes of selected earthquakes have shed new light on our understanding of seismic rupture propagation and stress relaxation and have identified the fundamental role that friction plays in earthquakes (see, e.g., Wald and Heaton, 1994; Cohee and Beroza, 1994; Cotton and Campillo, 1995; Beroza and Mikumo, 1996; Ide and Takeo, 1997). These models suggest a complexity of the rupture process that simple 2D or 3D models of rupture in a uniformly loaded medium may not explain.

An essential requirement to study dynamic faulting is an accurate and robust method for the numerical modeling of seismic sources. Two methods have been widely used for three-dimensional problems: one is the boundary integral equations (BIE) method pioneered by Das and Aki (1977) that has recently been improved by the removal of strong singularities (e.g., Cochard and Madariaga, 1994; Geubelle and Rice, 1995; Fukuyama and Madariaga, 1995, 1998; Bouchon and Streiff, 1997). These methods are excellent for the study of earthquake recurrence and the transition from transient accelerated fault creep to fully dynamic rupture propagation. However, at least in their current implementations, they cannot be used in heterogeneous media. The finite-difference (FD) method introduced by Madariaga (1976) and Andrews (1976) for the study of seismic ruptures and developed by numerous authors (e.g., Day, 1982a,b; Miyatake, 1992; Mikumo and Miyatake, 1995; Harris and Day, 1993) can be used to study rupture propagation in heterogeneous elastic media and are very efficient. The use of FD methods requires careful implementation of boundary conditions, in particular free surfaces, as shown by several au-

thors (see, e.g., Kosloff *et al.,* 1990; Ohminato and Chouet, 1997). Virieux and Madariaga (1982) encountered serious problems with the implementation of mixed boundary conditions (stress inside the rupture zone and slip outside it) in their staggered-grid velocity-stress FD method. There seem to be other implementations of the FD method that do not pose problems with boundary conditions (Day, 1982b, and personal comm., 1998). Recently, Olsen *et al.* (1995) and Olsen and Archuleta (1996) demonstrated the efficiency of the fourth-order formulation of the velocity-stress method (Levander, 1988) by computing wave propagation around a kinematically defined rupture in a large-scale 3D model. In this study, we extend their method in order to study dynamic rupture propagation on a planar shear fault embedded in a heterogeneous elastic half-space. For that purpose, we introduce a new way to impose mixed boundary conditions on a plane that coincides with one of the mesh planes. It would be possible in principle to simulate geometrically more complex ruptures, but problems of numerical instability are very likely to appear and are left for future work.

Rupture propagation on a major earthquake fault is controlled by the properties of the friction law on the fault. Friction controls the initiation, development of rupture, and the healing of faults. Laboratory experiments at low slip rates were analyzed by Dieterich (1978, 1979) and Ruina (1983), who proposed models of rate- and state-dependent friction, and by Ohnaka and Kuwahara (1990) and Ohnaka (1996), who concluded that their experiments could be explained with a simpler slip-weakening friction law. These two approaches to friction can be reconciled remarking that both models contain a finite-length scale that controls the behavior of the rupture front. Slip-weakening friction laws were introduced in dynamic rupture modeling by Andrews (1976) for plane (2D) ruptures and by Day (1982b) for 3D fault models. Both authors showed that slip weakening regularizes the numerical model of the rupture front, distributing stress and slip concentrations over a distance controlled by the length scale in the friction law. While these studies showed the need for a regularization mechanism, it was not clear how many grid points were needed to implement them in order to avoid using artificial damping or filtering of the slip-rate field. Proper regularization of the slip-rate field is essential to implement rate-dependent friction. Following Andrews (1976), we show that a relatively large number of points ($\geqq 4$) is needed to resolve slip rate near the rupture front.

In this article, we present and test the validity of our particular implementation of dynamic rupture propagation using the staggered-grid method. This implementation was used to compute spontaneous rupture propagation for the Landers earthquake by Olsen *et al.* (1997).

Elastic Shear Fault Model

We study numerical solutions of the 3D elastic-wave equation:

$$\rho \frac{\partial^2}{\partial t^2} \mathbf{u} = \nabla \cdot \sigma, \tag{1}$$

where $\mathbf{u}(\mathbf{x}, t)$ is the displacement vector field, a function of both position $\mathbf{x}$ and time t. and $\rho(\mathbf{x})$ is the density of the elastic medium. Associated with the displacement field $\mathbf{u}$, we have the stress tensor $\sigma(\mathbf{x}, t)$ defined by

$$\sigma = \lambda \nabla \cdot \mathbf{u}\mathbf{I} + \mu[(\nabla \mathbf{u}) + (\nabla \mathbf{u})^T], \tag{2}$$

where $\lambda(\mathbf{x})$ and $\mu(\mathbf{x})$ are Lamé's elastic constants. We can transform this system into a more symmetric velocity-stress formulation (Madariaga, 1976; Virieux and Madariaga, 1982; Virieux, 1986):

$$\rho \frac{\partial}{\partial t} \mathbf{v} = \nabla \cdot \sigma + \mathbf{f}$$

$$\frac{\partial}{\partial t} \sigma = \lambda \nabla \cdot \mathbf{v}\mathbf{I} + \mu[(\nabla \mathbf{v}) + (\nabla \mathbf{v})^T] + \dot{\mathbf{m}}. \tag{3}$$

where $\mathbf{v}(\mathbf{x}, t)$ is the particle velocity vector and $\mathbf{f}(\mathbf{x})$ and $\dot{\mathbf{m}}(\mathbf{x})$ are the force and moment rate source distributions, respectively.

Slip Boundary Conditions on the Fault

For simplicity and due to present limitations of the numerical method, we assume that the fault is a flat horizontal plane perpendicular to the z axis in the elastic medium. Due to frictional instability, a rupture zone can spread along the fault; let $\Gamma(t)$ be this rupture zone at time t. The kinematic inversion studies cited in the Introduction show that $\Gamma(t)$ will usually be a collection of one or more rupture zones propagating along the fault.

The main feature of a seismic rupture is that at any point $\mathbf{x}$ inside the rupture zone $\Gamma(t)$, displacement and particle velocities are discontinuous. Let

$$\mathbf{D}(\mathbf{x},t) = \mathbf{u}^+(\mathbf{x}^+,t) - \mathbf{u}^-(\mathbf{x}^-,t) \tag{4}$$

be the slip vector across the fault, that is, the jump in displacement between the positive and the negative side of the fault. The notation $\mathbf{x}^\pm$ indicates a point immediately above or below the fault, and $\mathbf{u}^\pm$ is the corresponding displacement. In the following, we assume that shear faults do not open up because of the strong normal stress component; that is, slip has only two components different from zero (i.e., $\mathbf{D} = [D_r, D_y, 0]$), but this restriction could be easily removed.

Slip is associated through the solution of the wave equation (3) to a change in the traction $\mathbf{T} = \sigma \cdot \mathbf{e}_z = [\sigma_{zx}, \sigma_{yz}, \sigma_{zz}]$ across the fault:

$$\Delta \mathbf{T}(\mathbf{x},t) = \Delta \boldsymbol{\Sigma}[\mathbf{D}] \quad \text{for} \quad \mathbf{x} \in \Gamma(t). \tag{5}$$

where $\Delta\boldsymbol{\Sigma}[\mathbf{D}]$ is a complex singular functional of $\mathbf{D}$ and its time and space derivatives. The operator $\Delta\boldsymbol{\Sigma}$ has to be com-

puted explicitly in the BIE methods (see, e.g., Geubelle and Rice, 1995; Fukuyama and Madariaga, 1995, 1997) but not in FD because in this case $\Delta\mathbf{T}$ is obtained numerically. In fact, all we need is a numerical procedure that computes the stress change $\Delta\mathbf{T}$ given the slip distribution $\mathbf{D}$ at earlier times. The boundary condition in (5) imposes no a priori conditions on the signs of neither $\Delta\mathbf{T}$ nor $\mathbf{D}$, except that there should be no interpenetration of matter.

Friction Laws

The main assumption in seismic source dynamics is that traction across the fault is related to slip at the same point through a friction law that for our purposes can be expressed in the functional form

$$\mathbf{T}(\mathbf{D},\dot{\mathbf{D}},\theta_i) = \mathbf{T}_{\text{total}} \quad \text{for} \quad \mathbf{x} \in \Gamma(t). \tag{6}$$

Friction $\mathbf{T}$ is a function of at least slip, but an increasing amount of experimental evidence shows that it is also a function of slip rate $\dot{\mathbf{D}}$ and several state variables denoted by θ_i, $i = 1 \ldots N$. For more details, see Dieterich (1978, 1979), Rice and Ruina (1983), but see also Ohnaka (1996) for an alternative point of view.

The traction that appears in friction laws is the total traction $\mathbf{T}_{\text{total}}$ on the fault that can be expressed as the sum of a preexisting field stress $\mathbf{T}^0(\mathbf{x})$ and the stress change $\Delta\mathbf{T}$ due to slip on the fault obtained from (5). The prestress is caused by tectonic load of the fault and will usually be a combination of purely tectonic loads due to internal plate deformation, plate motion, etc., and the residual stress field remaining from previous seismic events on the fault and its vicinity. In the rest of this article, we assume that the preexisting stress is known.

Using (5), we can now explicitly formulate the friction law on the fault (6):

$$\mathbf{T}(\mathbf{D},\dot{\mathbf{D}},\theta_i) = \mathbf{T}^0(\mathbf{x}) + \Delta\mathbf{T}(\mathbf{x},t) \quad \text{for} \quad \mathbf{x} \in \Gamma(t). \tag{7}$$

Friction as defined by (7) is clearly a vector. For the appropriate study of a shear fault, we need to write (7) as a system of two equations. In spite of the importance of friction for earthquake dynamics, it has rarely been studied for a fault that extends in two dimensions inside a 3D elastic medium. Here, following earlier work by Archuleta and Day (1980), Day (1982a,b), and Spudich (1992), we choose to use a very simple approach that will certainly have to be refined in the future, assuming that slip rate and traction are antiparallel; that is,

$$\mathbf{T}(\mathbf{D},\dot{\mathbf{D}},\theta_i) = -T(D,\dot{D},\theta_i)\mathbf{e}_V, \tag{8}$$

where $\mathbf{e}_v = \dot{\mathbf{D}}/\|\dot{\mathbf{D}}\|$ is a unit vector in the direction of instantaneous slip rate. With this assumption, the boundary condition reduces (7) to the special form

$$-T(D,\dot{D},\theta_i)\mathbf{e}_V = \mathbf{T}^0(\mathbf{x}) + \Delta\mathbf{T}(\mathbf{x},t) \quad \text{for} \quad \mathbf{x} \in \Gamma(t). \tag{9}$$

Figure 1 (*left*) shows the vector diagram implied by this equation. The only fixed vector in this diagram is the prestress that is known. Friction and slip rate are collinear but antiparallel. Stress change $\Delta\mathbf{T}$ is in general neither collinear with prestress nor with friction. We know of no other condition that can be applied to this diagram. Dissipation is insured by the antiparallelism of friction and slip rate. In order to compare with previous results, we also implemented a simpler version of friction that we call the "scalar boundary condition." We assume that slip is only allowed in the direction of the initial stress that is everywhere parallel to the x axis; that is, $\mathbf{T}^0(\mathbf{x}) = [T_x^0(\mathbf{x}), 0]$ and $\mathbf{D}(\mathbf{x}, t) = [D_r(\mathbf{x}, t), 0]$,

$$\Delta T_x(\mathbf{x},t) = T(D,\dot{D},\theta_i) - T_x^0(\mathbf{x}) \quad \text{for} \quad \mathbf{x} \in \Gamma(t). \tag{10}$$

This boundary condition, which may be graphically described as if the fault had "rails" aligned in the x direction, has been applied in many 3D source models starting with Madariaga (1976).

Both boundary conditions (9) and (10) require a friction law that relates scalar traction T to slip, its derivatives, and possible state variables. Although any realistic friction law can be implemented with our method, we use a very simple one used by Cochard and Madariaga (1994). In this friction law, slip is zero until the total stress reaches a peak value (yield stress) that we denote with T_u. Once this stress has been reached, slip D starts to increase from zero and $T(D)$ decreases linearly to zero as slip increases:

$$T(D) = T_u\left(1 - \frac{D}{D_0}\right) \quad \text{for} \quad D < D_0,$$
$$T(D) = 0 \quad \text{for} \quad D > D_0. \tag{11}$$

where D_0 is a characteristic slip distance. This decrease of friction with increasing slip is usually called slip weakening in rock mechanics (Ida, 1972; Ohnaka, 1996). This friction law has been used in numerical simulations of rupture (e.g., Andrews, 1976; Day, 1982b; Harris and Day, 1993). Slip weakening at small slip is absolutely necessary for the friction law to be realizable, otherwise stress σ_z becomes infinite at the rupture front, so that seismic ruptures would spread at either S, Rayleigh, or P-wave velocities until they stop. Of course, in numerical implementations, stress is never infinite so that rupture velocity is numerically limited. This is the so-called Irwin criterion described by Das and Aki (1977) and used by many authors since their publication. In the present work, we want to avoid numerical control of the rupture front by all means, thus we have studied, in detail, the values of D_0 that render the numerical method independent of grid size.

For large values of slip, on the other hand, slip rate becomes the dominant parameter as shown by Dieterich

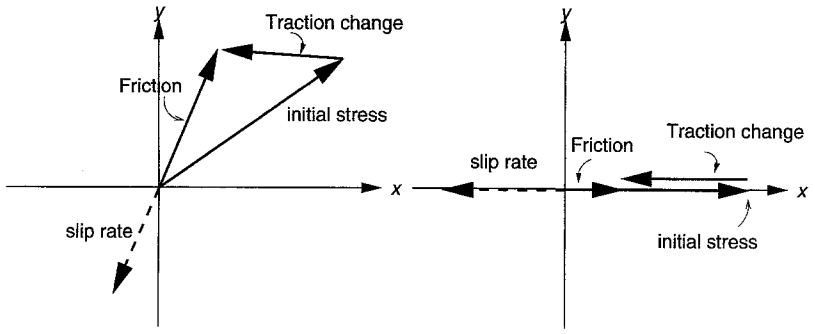

Figure 1. Diagram showing the relation between initial stress, slip rate, friction, and traction change for the vector (*left*) and scalar (*right*) approximations to friction on the fault plane. In the last case, traction change corresponds to the usual definition of stress drop.

(1978, 1979), Rice and Ruina (1983), and Ruina (1983). Although it is possible to use their friction laws in our numerical computations, this would require the integration of additional equations for the state variables. Because in this work we focus on the most essential aspects of rupture phenomenology in 3D, we will use a simplified friction that is a modification of the friction law used by Carlson and Langer (1989). For large slip D, we assume that friction increases when slip rate $\dot{D}$ decreases according to the friction law

$$T(\dot{D}) = T_s \frac{V_0}{V_0 + \dot{D}}, \tag{12}$$

where V_0 is a characteristic slip velocity and $T_s \leqq T_u$ is the limit of friction when slip rate decreases to zero. This behavior of friction is called *rate weakening* and has been observed in many materials (e.g., Dieterich, 1978, 1979; Rice and Ruina, 1983). Its applicability to seismic ruptures is much more controversial, although there is plenty of indirect evidence for its presence in seismic faulting. Heaton (1990) proposed that it was the cause of short rise times.

The actual friction law that we used in our simulations is a combination of both slip and rate-weakening friction; as for any value of D and $\dot{D}$, we choose the largest of (11) or (12). Instead of writing a complex expression, it is simpler to show the friction law graphically in Figure 2 in the form of a law where friction depends on the two state variables slip and slip rate. To sum up, in our simulations, rupture propagation is completely controlled by the complex nonlinear interaction of

1. the initial stress field $\mathbf{T}^0$ in (7);
2. the distribution of yield frictional resistance T_u in (11) and (12); and
3. the parameters D_0, T_S, and V_0 of the friction laws in (11) and (12).

Numerical Implementation

We solve the elastodynamic system of (3) in three dimensions with the fourth-order staggered-grid finite-difference method developed by Olsen (1994). This is an explicit implementation of the velocity-stress formulation in (3) using a fourth-order approximation to spatial derivatives and a second-order approximation to temporal ones. In this scheme, illustrated in Figure 3, stress and velocities are defined at alternating half-integer time steps. At time $t_N = N\Delta t$, particle velocity v is computed from previously calculated stress components. At the next half-time step $t_{N+1/2} = (N + 1/2)\Delta t$, stress σ is updated using the velocity field computed at time t_N. Thus, as time increases, velocities and stresses are computed at alternate times. Because stress and velocities are computed from (3) using centered fourth-order finite differences, the grid is also staggered in space as shown in Figure 3.

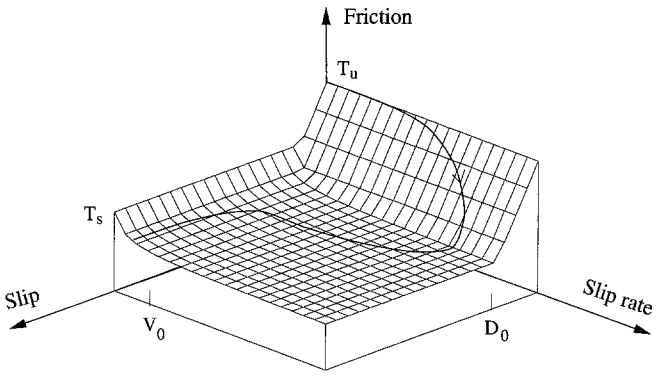

Figure 2. Slip- and slip-rate–dependent friction law. For values of stress less than the peak static friction (T_u), slip and slip rate are zero. Once slip begins, stress is a function of both slip and slip rate described by the friction surface $T(D, \dot{D})$. Slip weakening is measured by D_0; rate weakening, by V_0. The continuous curve shows the typical stress trajectory of a point of the fault.

The wave equation (3) is solved with homogeneous (i.e., $\mathbf{v} = 0$, $\sigma_i = 0$) initial conditions. All the waves that propagate in our model are generated by the fault itself. The conditions on the fault are the most important element of our numerical method and is explained in detail in the following section.

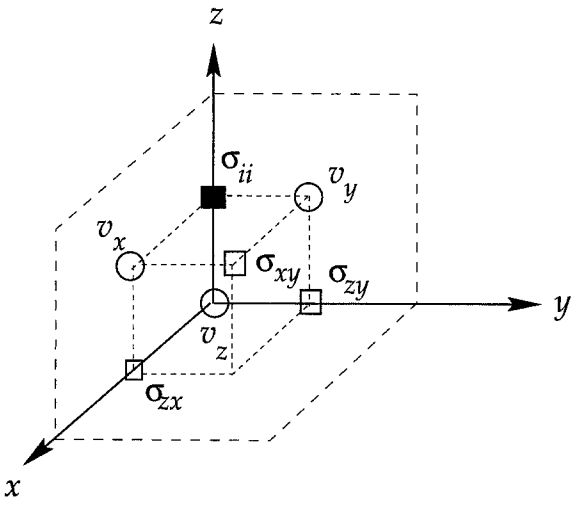

Figure 3. A cubic element of the 3D finite-difference grid used in the dynamic modeling of a planar shear fault. σ and **v** depict the components of the stress tensor and particle velocity, respectively.

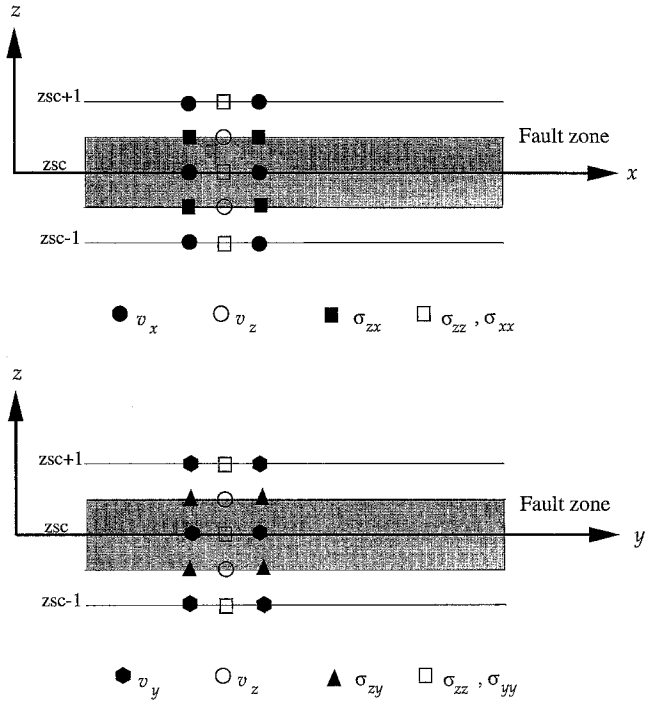

Figure 4. Vertical cross sections along x (*top*) and y (*bottom*) of the thick fault zone used in our numerical method. Note that the fault zone has the width of one grid spacing. The horizontal component of particle velocities v_x and v_y as well as the normal (σ_{ii}) and shear-stress components σ_{xy} (not shown) are staggered at integer grid planes zsc (center of the fault), $zsc + 1$, and $zsc - 1$. The vertical-component particle velocity v_z and shear-stress components σ_{zx} and σ_{zy} are staggered at half-integer grid points.

Numerical Implementation of Boundary Conditions

In the staggered grid used in our FD method, stresses and displacements cannot be computed at the same grid points, so that special care must be exerted in order to apply friction boundary conditions like (8). In earlier applications of the staggered-grid FD method to study rupture propagation (Virieux and Madariaga, 1982), the elastic medium was split in two by the fault plane, and symmetry about this plane was used. This led to a series of annoying problems, particularly near the crack tip where the boundary conditions could not be applied on the same grid plane ahead of and behind the rupture front. The problem remained even when slip-weakening friction laws were used (unpublished results). We have devised a new approach to the fault boundary conditions based on the use of a thick fault zone that spreads one-half grid cell to each side of the fault axis. As illustrated in Figure 4, we consider a one-grid element-wide fault zone centered around the plane $z = zsc$. It follows from the symmetries of a plane shear fault in a homogeneous medium that v_x and v_y are antisymmetric about the fault plane $z = zsc$, while v_z is symmetric about this plane. Similarly, the stress components σ_{zx} and σ_{zy} are symmetric about the fault plane $z = zsc$, while the normal stress components σ_{ii} and the shear stress σ_{xy} are antisymmetric with respect to $z = zsc$. The thick fault zone staggered-grid FD method preserves the symmetry of stresses and velocities across the fault. We have checked that this is valid both for the fourth-order FD method used here as well as for the second-order one, although the latter has much poorer resolution.

In the practical implementation, we impose the rupture zone boundary conditions in such a way that the symmetry of stresses and velocities about the fault plane are preserved:

1. If the fault is slipping, that is, if $\dot{\mathbf{D}} > 0$, we impose the boundary condition (9) (vector friction) or (10) (scalar friction) on the two stress planes $z = zsc \pm 1/2\Delta z$.
2. If the fault is locked, that is, if $\dot{\mathbf{D}} = 0$, $T(x, y, zsc) < T_u$, the boundary condition is applied directly on the fault plane, that is, $v_x(x, y, zsc) = v_y(x, y, zsc) = 0$, where v_x, v_y are the particle velocity components along the fault.

Thus, in order to preserve symmetry, stress and velocity boundary conditions are implemented differently. Because by construction $v_x(x, y, zsc)$ and $v_y(x, y, zsc)$ are always 0, we compute the slip rate $\dot{\mathbf{D}}$ between the walls of the fault in the following way:

$$\dot{\mathbf{D}}(x, y, zsc) = \mathbf{v}(x, y, zsc + \Delta z) - \mathbf{v}(x, y, zsc - \Delta z). \quad (13)$$

Finally, slip $\mathbf{D}$ is computed by straightforward numerical integration of the slip rate in (13).

In order to understand the practical implementation of the friction law, consider the state at time $t = t_N$. Velocity components are updated from the previous stress field at

time $t = t_{N-1/2}$, and slip rate on the fault is computed from (13) and integrated to obtain slip **D**. At the next half time step $t = t_{N+1/2}$, stress σ is computed everywhere. Then we apply the boundary conditions using the friction law defined by (11) and (12) and Figure 2.

Dimensional Analysis

In all our simulations, we used nondimensional variables. This has the advantage of clearly showing how different variables scale with stresses and distances. We choose the following dimensional variables:

- Distances along the fault are measured in units of Δx, the grid interval.
- Wave velocities are measured in units of β, the shear-wave velocity.
- Stress is measured in units of T_u, the peak frictional resistance (yield stress) in the friction laws described in (11) and (12).

All other dimensions are determined by these definitions. In particular,

- Time is measured in units of $\Delta t = H\Delta x/\alpha$, where α is the P-wave velocity. H is the so-called CFL (Courant–Friedrich–Lewy) parameter that controls stability of the numerical method. In our simulations, it was taken less than or equal to 0.43 in order to insure stability and good accuracy.
- Displacement is measured in units of $T_u/\mu \times \Delta x$.
- Particle velocities are measured in units of $T_u/\mu \times \beta$.

Slip and slip rate are normalized by $2T_u/\mu \times \Delta x$ and $2T_u/\mu \times \beta$, respectively. The factor of 2 is not really necessary, but we decided to follow the tradition in seismological publications. We also assume in the numerical computations that the P-wave velocity α is equal to $\sqrt{3}\beta$. Finally, D_0, the slip-weakening distance in (11), is measured in units of slip (i.e., $2T_u/\mu \times \Delta x$), and V_0, the rate-weakening parameter, is measured in units of slip rate (i.e., $2T_u/\mu \times \beta$).

It is important to remark that we used the more traditional choice Δx, the grid interval, as unit of length. We preferred Δx to a physical length such as the slip-weakening distance D_0 as unit of displacement because, as discussed later, the relation between D_0 and distances along the fault is dependent on load and rupture history.

Validation of the Numerical Method

Testing a numerical method for the solution of 3D spontaneous rupture along a planar fault is a difficult problem because the only known exact solutions for shear faults are the self-similar ruptures that start from a point (Kostrov, 1964: Burridge and Willis, 1969) and expand at constant rupture velocity with either a circular or an elliptical shape. Such solutions are unfortunately incompatible with friction models that contain an intrinsic length scale, because ruptures in such media can only start from a finite initial rupture patch. For this reason, we decided to validate the numerical method by studying a circular shear fault that breaks instantaneously and does not propagate. This problem was approximated by Brune (1970) and solved numerically assuming circular symmetry by Madariaga (1976). It is also representative for the initial asperity models discussed in the following section where we trigger rupture by a sudden "push" within a finite circular patch. The friction law plays no role in this simulation, our main purpose is to check that slip and stress are mutually consistent.

We simulated numerically the instantaneous rupture of a circular fault embedded in a homogeneous elastic medium of S-wave speed $\beta = 1$, P-wave speed $\alpha = \sqrt{3}$, and density $\rho = 1$. The fault has a radius of $30\Delta x$. We assumed a simple Coulombian friction (i.e., $D_0 = 0$ and $V_0 = 0$ with yield value $T_u = 1$). Prestress on the fault just before rupture was exactly $T_0 = T_u = 1$. Stress reduces instantly to zero at $t = 0$, so that the stress drop $\Delta\sigma$ is exactly 1 everywhere in the rupture zone. As shown by Brune (1970), this fault radiates a plane shear wave perpendicularly to the plane of the fault of amplitude $T_u/\mu\beta = 1$ in our nondimensional units.

In Figure 5, we show the numerical solution of slip computed on this instantaneously rupturing circular shear fault. At the top, we show slip as a function of time and radius along the x axis of the fault. The initial slope of all the slip functions is clearly equal to 1, as expected for the initial radiation according to Brune's (1970) model. After about 20 time units, the slip functions at the center of the fault show a break in slope corresponding to the arrival of the P stopping phase. After about 34 time units, the S stopping phase arrives, soon after which the fault stops slipping. Because we do not allow slip rate to change sign, the final slip overshoots the static solution, but overshoot for a circular shear fault is very small. Stress inside the fault adjusts very slowly to this additional stress drop. The final slip at the center of the fault is indicated with an arrow and matches very well the static value of $\pi/4\Delta\sigma/\mu \times r$, where r is the radius of the fault (see, e.g., Scholz, 1989). The bottom of Figure 5 shows the slip functions along the y axis; the solutions are similar to those on the top, but they are not exactly equal. It is interesting to remark that even for a simple instantaneous circular fault, there is no cylindrical symmetry around the center of the fault. This occurs because faulting is in the in-plane mode (mode II) along the x axis and in antiplane mode (mode III) along the y axis. These results show that our numerical method is stable and produces smooth slip functions that reproduce many of the known properties of the simple instantaneous circular crack model proposed by Brune (1970).

Spontaneous Rupture of a Localized Asperity

We illustrate spontaneous rupture starting from a circular asperity ready to break, surrounded by a fault surface with a lower stress level. These conditions are very similar to those used by Day (1982b) and Das (1981) to start rupture. There are two main reasons to proceed this way: First, if the

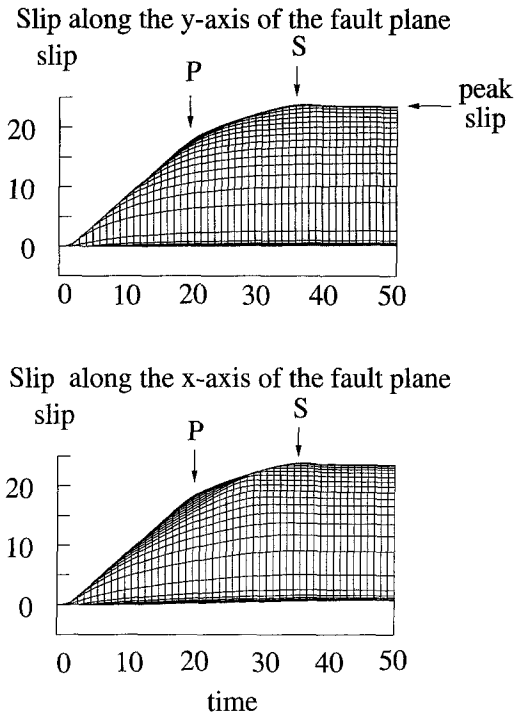

Figure 5. Slip as a function of time for an instantaneous circular fault. Each curve represents the slip function at a different point along a radius of the fault. Slip along the x axis (*top*) and the corresponding slip functions along the y axis (*bottom*). The arrows indicate the arrival of P and S stopping phases at the center of the fault. The horizontal arrow to the right of the source functions indicates the theoretical slip at the center of a circular shear fault with the same stress drop.

asperity is too small, rupture will start and stop immediately. For rupture to expand, stress must be high over a finite zone, sometimes called *the minimum rupture patch.* Once rupture has started from this asperity, it will grow or stop depending on the values of the stress field inside and outside the asperity and the constants D_0 and V_0 of the friction law in (11) and (12). A full exploration of the parameter space will be subject of future work, but the parameters used in our simulations were chosen so as to push the rupture beyond the asperity (this is equivalent to using the so-called sigma parameter of the friction law used by Langer *et al.* 1996). As shown by Rice and Ben-Zion (1996), this initial kick is not needed if one uses one of the Dieterich–Ruina friction laws that contain a time-dependent relaxation mechanism and if one uses a numerical procedure that models the slow buildup of applied stresses over times that are much longer than the rupture time. Second, if the stress field were uniform, rupture would occur instantaneously or grow at the maximum possible velocity from an arbitrary point on the fault. This is unrealistic and not supported by observations. Thus, we assume that fault rupture must occur at stress levels that are below the yield stress except for a small number of isolated asperities. In the following examples, we assume that there is only one such asperity even though rupture starting from several locations is possible (e.g., Day, 1982b; Olsen *et al.*, 1997).

Scaling of Rupture with the Slip-Weakening Distance D_0

An essential requirement for an accurate numerical method is that the numerical solution becomes independent of grid size beyond the use of a certain number of grid points per wavelength. In our problem, the shortest physical distances are the radius of the asperity R and the width of the rupture front. The latter depends on the slip-weakening distance D_0 as shown by Ida (1972) and Andrews (1976). For 2D faults and for the slip-weakening law (11), this width, L_c, is

$$L_c = \frac{4\mu}{3\pi} \frac{T_u}{T_{\text{ext}}^2} D_0. \tag{14}$$

We have assumed as in (11) that the residual friction at high slip rates is $T_f = 0$. This expression is valid for a constant stress level T_{ext} outside the asperity. For a stress distribution that scales only with the size of the grid, the fault scales with D_0. However, it would be convenient to scale our numerical computations by L_c instead of D_0, but unfortunately, (14) depends on the load through the initial stress field T_{ext}. If this external stress varies spatially, the denominator has to be replaced by a complex expression that contains the stress intensity. Furthermore, (14) is only valid asymptotically, when the crack tip is very sharp. For these reasons, we decided to use Δx and not D_0 as length scale in our numerical simulations.

In order to study the convergence of the numerical method as the grid size is refined, we study the scaling of a simple circular asperity keeping all the parameters constant except the grid size and D_0. Stress inside the asperity is $T_{\text{asp}} = 1.8 \times T_u$, $T_{\text{ext}} = 0.8 \times T_u$, and $H = 0.35$. Replacing T_{ext} in (14), we find that $L_c = 1.36 \times D_0$. Figure 6 shows snapshots of the slip rate as a function of position on the fault at equivalent instants of time. Because we use Δx as the scaling distance, we have to increase both the radius of the asperity R as well as the time of the snapshot for increasing values of D_0. The four figures show from the top left snapshots for $t = 140$ ($D_0 = 2$, $R = 3$), $t = 280$ ($D_0 = 4$, $R = 6$), $t = 420$ ($D_0 = 6$, $R = 9$), and $t = 560$ ($D_0 = 8$, $R = 12$). The external rectangles define the size of the grid, 256×256 for D_0 from 2 to 6 and 300×256 for $D_0 = 8$. Note the scaling of the figures; that is, the snapshot for $D_0 = 8$ is precisely twice as large as as that for $D_0 = 4$. Clearly, the degree of resolution improves as D_0 increases.

From a close examination of these snapshots and several others, we concluded that the solutions for the thick fault boundary conditions implemented in a fourth-order staggered-grid method are contaminated by numerical noise

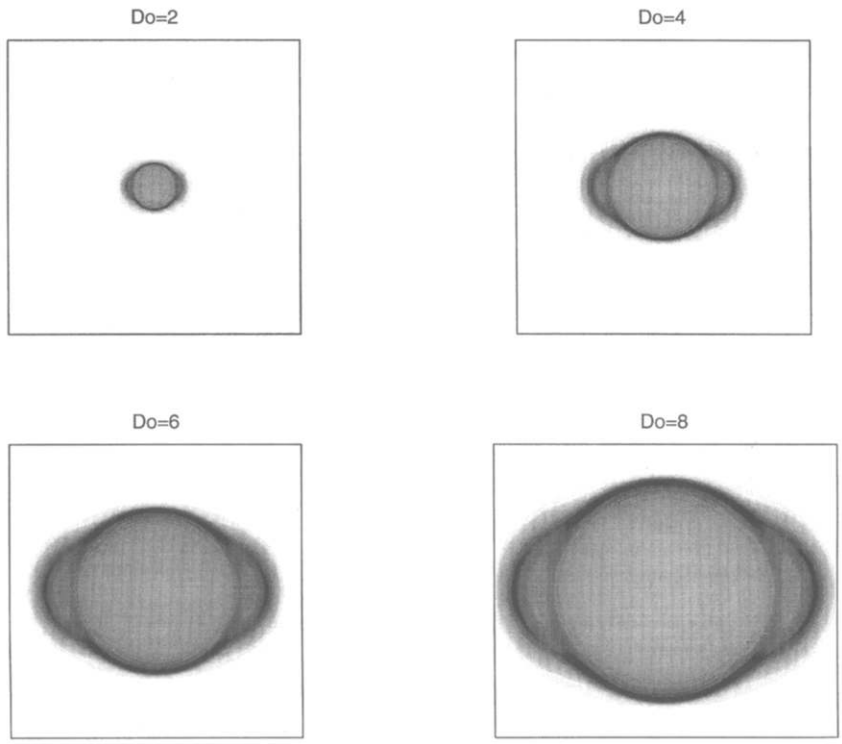

Figure 6. Scaling of rupture at constant load for spontaneous rupture starting from an overloaded asperity. The four snapshots show the distribution of slip rate on the fault at equivalent times for four different values of D_0. The initial asperity radius R as well as the instant of time of the snapshot all scale with D_0. (*top left*) $D_0 = 2$, $R = 3$, and $T = 140$; (*top right*) $D_0 = 4$, $R = 6$, and $T = 280$; (*bottom left*) $D_0 = 6$, $R = 9$, and $T = 420$; and (*bottom right*) $D_0 = 8$, $R = 12$, and $T = 560$.

when $D_0 < 4$ and that numerical simulations are stable and reproducible for $D_0 > 4$ ($L_c > 5.44\Delta x$). For 3D simulations, this is a rather large number that requires the use of very dense grids for accurate simulation of spontaneous rupture. Andrews (1976) studied 2D spontaneous rupture with the same slip-weakening law as ours using a second-order FD method. He reported stable results for $L_c = 10 \times \Delta x$, although certain models used $L_c = 5 \times \Delta x$ in nondimensional units. Despite the use of a value of T_{ext} different from ours, his L_C is quite equivalent to ours. Detailed comparison is difficult with the 3D simulations of Day (1982b) who expressed L_c in terms of D_0, not Δx as here.

Spontaneous Growth of Rupture

We use the simple 3D fault model of the previous section (initial stress distribution symmetric about the origin) to study the spontaneous growth of rupture. Rupture resistance, represented by T_u and D_0, is perfectly uniform. This model is not unlike that of Kostrov (1964) or Burridge and Willis (1969). The main differences are that, as previously explained, we initiate the rupture from a finite asperity and that the rupture velocity is not a prescribed constant but determined from the friction law. Our solutions are not self-similar and, as already illustrated by Das (1981), Day (1982b), Virieux and Madariaga (1982), and others, spontaneous ruptures do not maintain simple elliptical shapes as they grow.

To illustrate the resolution and stability of the numerical method, we used an asperity with a radius $R = 10\Delta x$. The initial stress was $1.6 \times T_u$ inside and $0.5 \times T_u$ outside the asperity. The excess stress in the asperity is enough to give a strong initial kick to the rupture so that it propagates away from the asperity. For smaller values of the initial stress or radius of the asperity, the rupture would simply stop. The slip-weakening parameter was $D_0 = 4$ in nondimensional units (see equation 11) and $H = 0.35$. The final stress inside the fault is close to zero, obtained numerically from the simulation.

Figure 7 shows slip and stress distributions on the fault plane as a function of time and position along the x axis of the fault (the in-plane, or mode II direction). We observe that rupture starts from a zone around the center of the fault and then grows bilaterally at a slightly increasing rate. The slip function at the bottom resembles that of a self-similar fault but has a bump near the center of the fault. This localized excess slip is the most characteristic feature of faults that start from an initial asperity. Because this initial asperity forms spontaneously on a fault where the friction law has a characteristic length ($D_0 = 4$ in our particular friction law), we expect most slip functions to have such a feature. Nat-

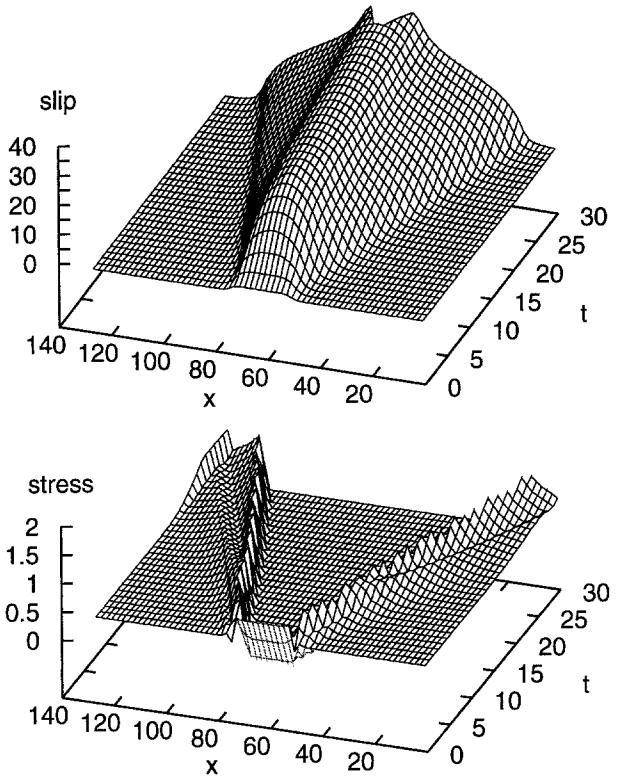

Figure 7. Slip (*top*) and stress (*bottom*) as a function of radius and time for a circular rupture growing spontaneously after the instantaneous break of an overloaded initial asperity. The radial section was computed along the longitudinal (x) axis of the fault. Rupture along this line is dominated by the in-plane stress. The ridge-shaped part of the slip is the excess slip due to large stress drop inside the asperity. Note the shear wave propagating ahead of the rupture front in the stress field.

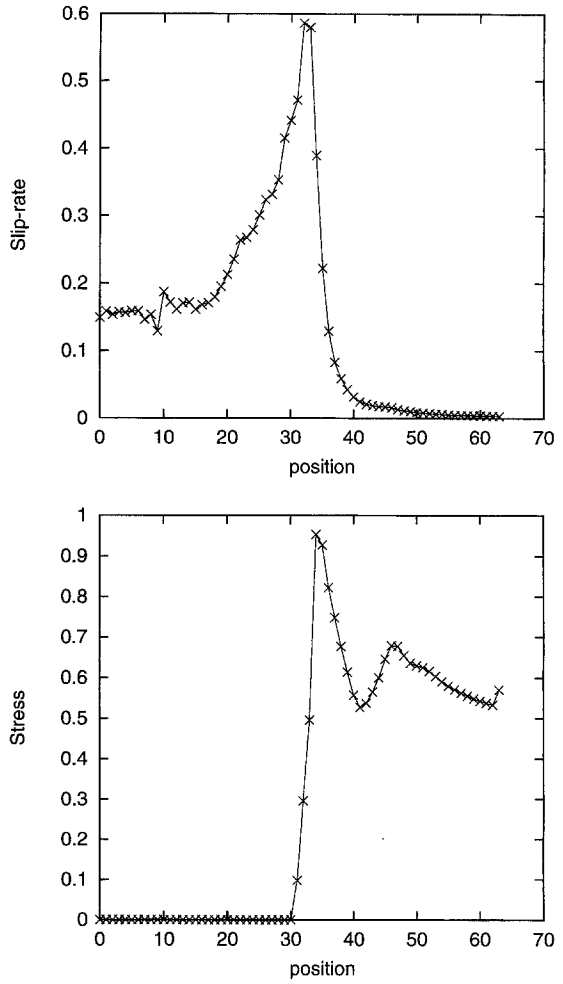

Figure 8. Resolution of the friction law, illustrated by the slip rate (*top*) and stress (*bottom*) as a function of position along the longitudinal (x) axis of the model shown in Figure 7, starting at the center of the fault. The crosses show the actual values computed numerically for $D_0 = 4$. The shear-stress wave is clearly seen as a bump ahead of the stress concentration due to the rupture front.

urally, if the initial asperity is small compared to the full size of the rupture, the bump will become insignificant, and the slip functions (Fig. 7) become similar to those of an elliptical crack.

Although stress (Fig. 7) is sharply concentrated around the rupture front, it does not contain the local oscillations that are frequently observed in low-resolution simulations. The strong ridgelike phase that is observed ahead of the rupture front is the S wave. As in the 2D simulations by Andrews (1976), the stress field has a peak that moves at the shear-wave speed. Andrews showed that when the stress field outside the fault is sufficiently strong, the rupture front becomes unstable, and the rupture jumps to the shear-wave speed. We show an example of this in a later section. Inside the fault, stress remains zero during the entire rupture process because we omitted any velocity weakening in these simulations.

In order to understand the accuracy of the numerical solution of the friction law (11), we show in Figure 8 the slip rate (*top*) and stress (*bottom*) distributions as functions of position along the longitudinal axis of the fault (the in-plane direction). We clearly observe the bump associated with the S wave, and the stress distribution closely resembles that determined by Andrews (1976) for a two-dimensional in-plane crack. The section was computed at a nondimensional time $t = 200$; at this time, the rupture front extends from grid points 30 to 35. For this simulation, we used $H = 0.35$, $D_0 = 4$, $T_{\text{ext}} = 0.5 \times T_u$, and the initial asperity had a nondimensional radius of $R = 10$. The stress field around the crack tip shown in Figure 8 confirms the scaling of the rupture with D_0 as discussed in the previous section, as it clearly shows that stress relaxes over a distance of about 5 grids. The peak of the S wave is at position 48 as expected because the S wave advances 1 grid point every 5 nondimensional time units for a CFL parameter of 0.35. The S wave emanates from the edge of the asperity at $x = 10$. In these figures, we used no artificial damping or filtering so

that, except for the low-amplitude numerical noise in the velocity field, the friction law is well resolved numerically. Because we compute slip rate between points located 1-grid interval away from the fault, slip rate begins to increase very slowly starting from the S wave. The oscillations in the slip-velocity fields are due to the jump of the rupture front from one grid point to the next. Compared to slip-rate fields computed in previous numerical simulations, we observe that the oscillations are satisfactorily damped by the use of a finite slip-weakening distance in the friction law. The overall quality of our simulations is similar to that obtained by Andrews (1976) and others in two-dimensional rupture simulations.

Spontaneous Rupture on a Finite Fault

In this section, we study the propagation of rupture away from the circular asperity presented in the previous section and the arrest of rupture when it reaches unbreakable boundaries of the fault. The main purpose of these studies is to show the role of stopping phases and healing phases for simple geometries, subjects that were first explored by Day (1982b) and Das and Kostrov (1983). We also briefly demonstrate that the numerical method proposed here can handle rate-dependent friction laws and vector friction, two important subjects of recent research in earthquake dynamics.

Circular Fault

We model a circular fault of radius $50 \times \Delta x$, starting from a concentric asperity of radius $6 \times \Delta x$, $D_0 = 4$; stress inside the asperity was $1.2 \times T_u$ and $0.8 \times T_u$ outside. Snapshots of slip rate are shown in Figure 9 at several successive instants of time. Time is measured in units of $\Delta t = H\Delta x/\alpha$, where $H = 0.35$ as discussed earlier. From time steps $t = 17.5$ to 35, rupture is taking place inside the asperity and propagating away from the asperity for $t > 52.5$. We observe that rupture becomes spontaneously elongated in the vertical direction, which is also the direction of the initial stress. Thus, as already remarked by Das (1981) and Day (1982b), rupture tends to grow faster in the in-plane direction, which is dominated by mode II.

At time $t = 87.5$, rupture in Figure 9 has reached the unbreakable border of the fault in the in-plane direction, and at time $t = 105$, the stopping phases generated by the top and bottom edges of the fault are moving toward the center of the fault. The snapshots after $t = 122.5$ show stopping phases propagating inward from all directions. The slipping patch in darker color is now elongated in the antiplane direction, which is due to slower healing. At time $t = 140$, the in-plane stopping phases (moving in the vertical direction) have already reached the center of the fault and crossed each other. In the last two snapshots, rupture continues in a small patch near the center of the fault that coincides with the initial asperity. However, slip rate has decreased to such small values that it is very likely contaminated with numerical noise.

Rectangular Fault

In the second set of simulations, we studied a model that starts in the same way as the circular fault from an overloaded asperity. However, here the unbreakable barriers force it to expand in essentially one direction along a rectangular fault. We build this model as a prototype of rupture along a shallow strike-slip fault and use the same values for the friction laws as those for the circular crack simulation. Here, $H = 0.35$, slip-weakening distance $D_0 = 4$, initial stresses inside and outside the asperity were $T_{\text{asp}} = 1.2 \times T_u$ and $T_{\text{ext}} = 0.8 \times T_u$, respectively, and the radius of the initial asperity $R_{\text{asp}} = 6 \times \Delta x$. For the rate-weakening simulations, we used $V_0 = 0.01$ and $T_s = T_u$.

Figures 10 and 11 show snapshots of the slip rate on the fault plane for simulations using slip-weakening friction and slip- and rate-weakening friction, respectively. The prestress on the fault is directed along the vertical (long) axis of the fault. In the simulation with slip weakening but no rate weakening (Fig. 10), we see the rupture emerging from the asperity with relatively slow healing (long wake trailing from the front). Rupture starts out slowly, accelerates toward the S-wave speed, and at a mature stage, near time $t = 80$, suddenly "jumps" to the P-wave speed. The transition to super-shear rupture speeds is an instability that develops from the in-plane direction and spreads laterally along the rupture front producing a "bulge" observed in the snapshots after $t = 80$. Stopping phases emitted from the edges of the fault clearly control the duration of slip as shown in snapshots at $t = 120$ through 160. In the snapshot at $t = 160$, the stopping phases have reached the center of the fault just below the time label 160.

The situation is quite different when we use a rate-dependent friction law, where the slip rate tends to concentrate in narrow patches (Fig. 11). Compared to Figure 10, the rupture front is narrower and clearly delineated. Well before the arrival of stopping phases from the edges of the fault, slip rate has become very small near the center of the asperity. Rupture takes the shape of a band. As time increases and rupture is controlled by the edges of the fault, the rupture front becomes narrow and localized. This is similar to the behavior predicted by Heaton (1990).

The other major difference introduced by rate-dependent friction is that the stress becomes extremely heterogeneous behind the narrower rupture front. It appears that the rupture leaves a wake of complexity after its passage. This complexity is apparent in the distributions of both stress drop (Fig. 12, *top*) and slip (Fig. 12, *bottom*). As is well known, the stress field is related to the spatial gradient of slip, so that heterogeneity is enhanced for the stress drop. Finally, note that the faster healing caused by rate-weakening friction decreases the final slip significantly.

Vector Friction

So far, we have allowed slip to occur only in the direction of the prestress. This produces locally large stresses in

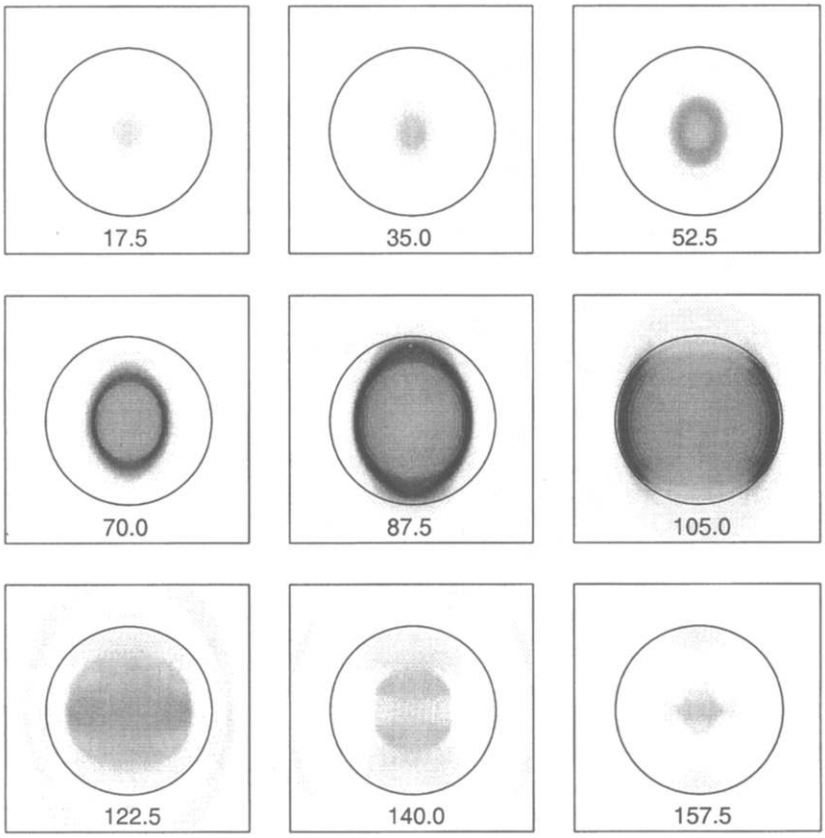

Figure 9. Snapshots of slip rate at successive instants of time for the spontaneous rupture of an overloaded asperity inside a circular fault (solid line). The nondimensional time for each snapshot is shown below each picture.

the direction perpendicular to the initial stress in order to force slip in the longitudinal direction. If we remove this strong restriction, slip is no longer parallel to the initial stress. Figure 13 shows a comparison between snapshots of the unidirectional slip rate (scalar friction approach) and the equivalent ones with slip allowed in any direction on the fault (vector friction approach). We used the same parameters as those for the simulation shown in Figure 10 (i.e., no rate weakening). The comparison shows that the two cases are very similar; that is, slip predominantly occurs along the prestress. The largest deviations occur near the rupture front and the edges of the fault. Note that healing appears slightly slower (i.e., longer tail trailing from the front) for the vector friction. However, this difference is likely due to the use of the same healing criterion for the two cases, that is, reversal of the slip rate in the direction of the prestress. In the future, healing for the vector friction will have to be modified to account for direction as well as magnitude of the slip-rate vector.

Discussion

Modeling of spontaneous seismic ruptures requires accurate numerical schemes with low dispersion and spatial resolution that allows the rupture front to be discretized by a sufficient number of grid points. Several versions of the finite-difference method have been proposed in the literature for the study of 3D spontaneous seismic ruptures by, among others, Virieux and Madariaga (1982), Day (1982b), and Mikumo and Miyatake (1992). In this article, we proposed a simple internal boundary condition for the modeling of a flat fault in the fourth-order staggered-grid method developed by Olsen (1994). Both slip-weakening and rate-dependent friction laws can be studied with a thick fault model, in which the internal boundary conditions on the fault are applied on two rows of cells surrounding the fault. It is very likely that the particular version of the boundary conditions we used can be improved (Stefan Nielsen, personal comm., 1998), as long as fourth-order accuracy is maintained near the fault. It appears that the reason why second-order staggered-grid FD schemes by Virieux and Madariaga (1982) were found to be inaccurate for the study of spontaneous rupture was the way in which they imposed boundary conditions inside and outside the rupture zone on the fault. We verified that the thick fault zone works both for second-order and fourth-order velocity-stress FD methods. However, in this article, we have used only the fourth-order method because it has a strong advantage over the second-order one in

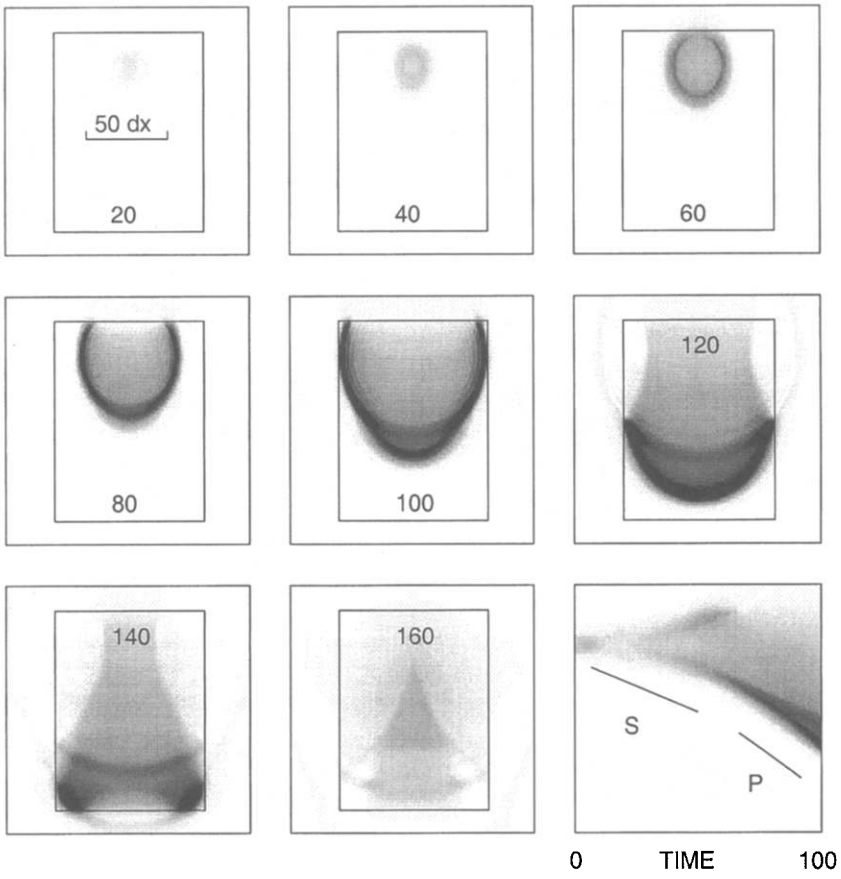

Figure 10. Snapshots of slip rate at successive instants of time for the spontaneous rupture of an overloaded asperity inside a rectangular fault (solid line). No velocity-weakening friction is included. The nondimensional time is listed for each snapshot. The lower right panel shows the slip rate versus time along a line in the in-plane direction intersecting the asperity. The slope of the slanted lines depicts the *P*- and *S*-wave velocity.

terms of the number of grid cells required per wavelength. We showed that accurate results can be obtained for $D_0 = 4$ or larger in nondimensional time units.

The use of symmetries necessary to impose the boundary conditions has the obvious limitation that this technique cannot be easily extended to study curved faults or faults slanted with respect to the finite-difference grid. On the other hand, our method can include free-surface boundary conditions, stratified media, and localized heterogeneities without any changes. Olsen *et al.* (1997) have, for instance, used this technique to model the 1992 Landers earthquake with a realistic crustal model.

The aim of this study was limited to the validation of numerical simulations through the study of simple rupture models that contain well-known properties of seismic ruptures in three dimensions. Except for the instantaneous rupture of a circular fault, none of the problems studied here has an exact solution for comparison. For this reason, we studied simple models that have already been discussed in the literature by many authors (see, e.g., Kostrov and Das, 1989, for a review). Our rupture simulations use a much larger number of grid points than in most previous models and are thus expected to be more accurate. It is therefore encouraging to see that we reproduce many known properties of shear faults. A problem we encountered in trying to compare our simulations with previous results is that the values of grid spacing and the slip-weakening distance were not always reported or were too coarse.

Among the properties of faulting that we reproduced successfully is the lack of cylindrical symmetry of shear faulting. This loss of symmetry was discovered by Kostrov (1974), who emphasized the difference of stress intensities along the antiplane and in-plane borders of the fault. Elliptical self-similar faults were studied by Burridge and Willis (1969) and others. The initial stress field introduces a fundamental anisotropy of rupture speeds for sharp shear cracks: stress intensities are higher in the antiplane (mode III) direction than in the in-plane (mode II) direction, suggesting faster growth in the antiplane direction. In our numerical simulations, this occurs only when $D_0 < 0.5$, but in

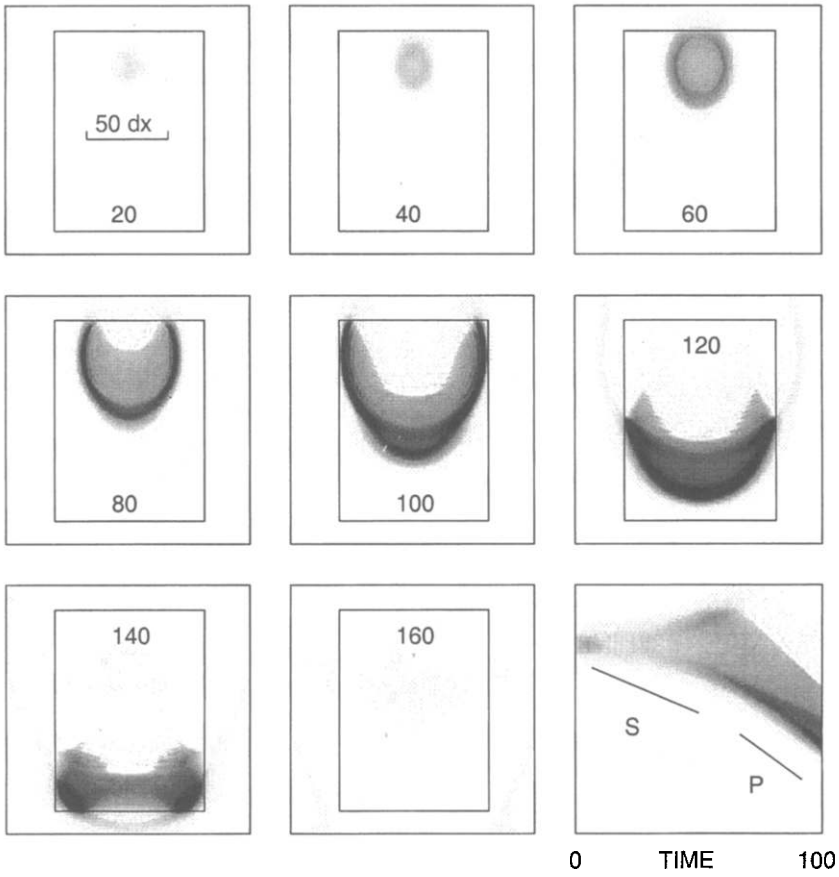

Figure 11. Same as Figure 10 but with velocity-weakening friction included in the simulation.

this case, the numerical solution does not model the rupture front accurately, and rupture is numerically controlled. When the grid resolution is sufficiently large (i.e., for $D_0 > 4$ in nondimensional units), ruptures always grow faster in the in-plane direction than in the antiplane one as observed by Day (1982b). The reason for this is the presence of a peak in stress that moves at the shear-wave speed. This peak exists only in the in-plane direction because vertically polarized shear waves have an extremum of the radiation pattern in this direction [see Fukuyama and Madariaga (1998) for further discussion in the context of modern displacement boundary integral equations]. For finite D_0, the rupture front is "pulled" by the stress concentration at the S wave, as is clearly observed in Figure 7. As proposed by Andrews (1974) for plane cracks and by Day (1982b) for 3D faults, rupture velocity tends to become super shear in the in-plane direction when the ratio of ambient stress outside the fault to peak stress is high. According to Andrews (1974), an in-plane rupture front becomes unstable and jumps to super-shear speeds when this ratio is of the order of 80%. In terms of the ratio S of Das and Aki (1977), transition to super-shear speeds occur when $(1 + S)^{-1} \cong 0.8$ or $S = 0.25$. This in in full agreement with the results reported by Day (1982b) in his Figure 4. In our high-resolution images shown in Figure 8, we clearly observe that the transition to super-shear speeds spreads laterally along the rupture front. Detailed study of the stress and slip-rate fields in the area between the shear wave and the rupture front shows that the instability is accurately modeled numerically, without contamination of numerical noise. The transition to super-shear speeds is perfectly stable for the four different grid resolutions shown in Figure 8. Such super-shear transition is rarely observed in actual earthquakes, except for local bursts of fast rupture for the 1979 Imperial Valley earthquake (Archuleta, 1984). Two explanations for the small number of observations of super-shear rupture speeds seem possible to us: either stress distributions in the fault zone are very heterogeneous and only isolated patches of the fault are highly stressed (Day, 1982b; Olsen *et al.*, 1997) or strongly rate-dependent healing behind the rupture front inhibits super-shear speeds (Cochard and Madariaga, 1994). For a number of reasons, including the results from the simulation of the Landers earthquake by Olsen *et al.* (1997), we prefer the first explanation where the distribution of prestress determines the propagation of the rupture front and produces rapid healing of slip.

Rupture initiation occurs over a patch of a size that is related to the slip-weakening distance D_0. Without a highly

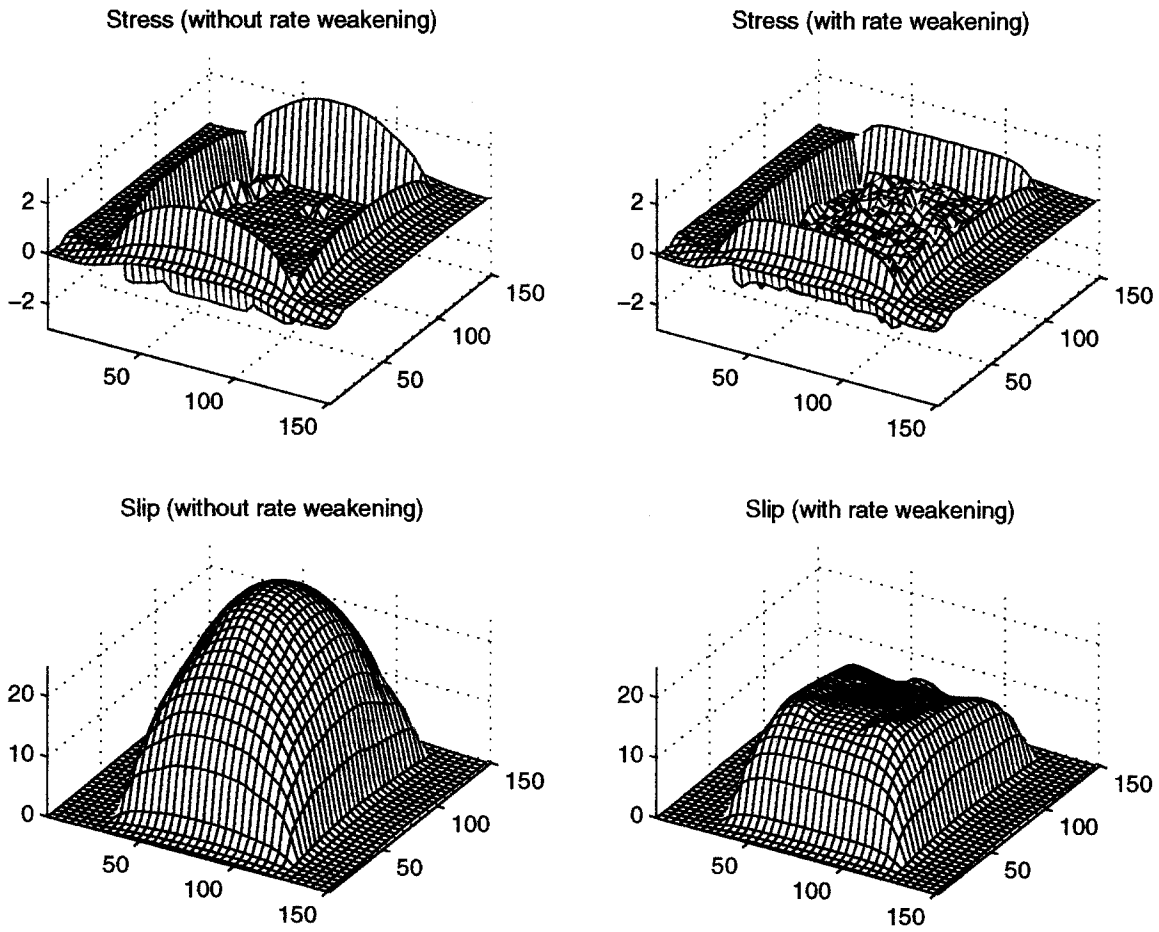

Figure 12. Final stress without (*top left*) and with (*top right*) rate weakening, and final slip without (*bottom left*) and with (*bottom right*) rate weakening, for the simulations shown in Figures 10 and 11. The plots clearly show a decrease in slip as well as the development of stress heterogeneity inside the fault due to rate weakening.

prestressed patch larger than such critical size, rupture will start and die immediately. Although we can determine numerically the size of the asperity needed to start rupture for a given value of D_0, we did not manage to derive a simple expression that takes into account also the prestress outside the asperity. In principle, rupture development is determined by the stress concentration on the rupture front, propagating as the prestress times some power of the radius of the asperity. Simple asymptotic numerical analysis suggests that this power should be 1/2, whereas our numerical experience indicates a value closer to 1. Clearly, this point needs further theoretical scrutiny in order to understand rupture under finite fracture energy. The problem is that when rupture emerges from the asperity, the asymptotic shape expected from crack theory is not yet fully developed. A possible reason is that, as the fault reaches the critical size, slip rates are not large enough to generate seismic waves. The way the rupture is initiated strongly influences its subsequent development (i.e., generation of heterogeneity) as stressed by Langer *et al.* (1996), Madariaga and Cochard (1996), and Rice and Ben-Zion (1996). In our simulations, we triggered ruptures by a sudden break of a finite zone on the fault (an "asperity"). The rupture initiation problem will be a strong focus of our future research.

An important feature of friction laws that we briefly explored for a rectangular fault is their sensitivity to slip rate. It has been demonstrated in a number of experiments on very different materials that, at least at low slip rates, friction is rate sensitive, decreasing when slip rate increases. From a theoretical point of view, several authors, starting with Carlson and Langer (1989), showed that if friction weakens with slip rate, slip and stress heterogeneity may develop even on a perfectly flat, uniform fault. This is a somewhat controversial subject that needs to be studied in three dimensions [see, e.g., Langer *et al.* (1996), Madariaga and Cochard (1996), Rice and Ben-Zion (1996) for different points of view]. A strong limitation of numerical methods for this purpose is the noise that appears behind the healing "front." This noise occurs because of geometrical effects in the rectangular grid and produces in extreme cases a sort of "scintillation" of the fault plane where slip rapidly starts and stops. This is likely due to "healing noise": when slip rate

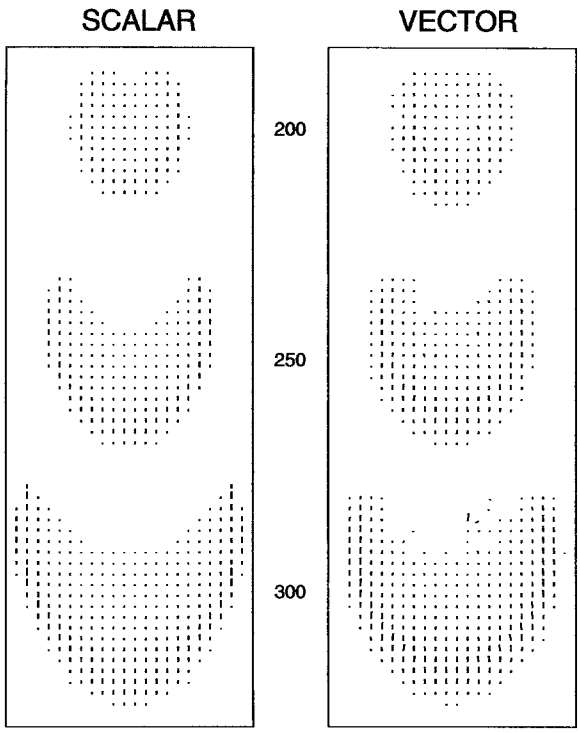

Figure 13. Snapshots of the slip rate on a rectangular fault using scalar (*left*) and vector (*right*) boundary conditions for the friction. For clarity, only slip-rate vectors where $\dot{D} > 0.25$ are plotted for the slipping areas on the fault. The nondimensional time is listed for each of the three snapshots.

tends to change sign very frequently, neighboring points of the fault heal at slightly different times. We expect that the use of more sophisticated friction laws with state variables and a finer discretization of the fault may produce smoother results. Finally, another currently undertaken problem (see, e.g., Ide and Takeo, 1997) is to determine the friction laws by inversion of recorded ground motion. Results of such analysis can be used to set important guidelines for future inversion attempts to capture the physics of earthquake rupture but may require very accurate high-resolution simulation methods without artificial numerical damping. This is an area where our FD method should excel.

Our staggered-grid velocity stress FD method can be improved and extended in several ways. Foremost, our study was limited to a single planar fault. However, we expect no substantial problems for the implementation of boundary conditions for two or more parallel fault strands. The method presented is presently limited to planar faults, while the much more challenging implementation of more realistic geometries is left for future work. Such configuration would allow the study of fault interactions in three dimensions (Harris and Day, 1993). Also, while our method is tested for simple slip- and rate-weakening boundary conditions on the fault, it can in principle be extended to use any realistic friction law. It would be possible, for example, to use the rate- and state-dependent friction laws of Dieterich and Ruina. If the use of vector friction is considered critical, our suggested healing criteria should be improved.

Conclusions

We have shown that the fourth-order staggered-grid velocity-stress finite-difference method can be used very effectively to study spontaneous rupture propagation in a realistic fault model embedded in a 3D elastic medium. We show that the use of a simple slip-weakening model containing a length scale is able to regularize the rupture front. The solutions for our fault boundary conditions scale with D_0 and are stable and reproducible for D_0 greater than 4. This regularization eliminates undesirable oscillations in the stress and slip-rate fields in the vicinity of the rupture front. It therefore allows simulation of realistic rate-, slip-, and state-dependent friction laws without any numerical damping. After initiation from a finite initial patch, the spontaneous rupture accelerates to a speed close to that for the S waves. If the rupture resistance level is below a critical value, the rupture speed jumps to that for the P waves, starting along the in-plane direction. The use of rate-weakening friction tends to increase the rupture resistance, thereby inhibiting the transition to super-shear rupture velocities. Healing occurs by stopping phases from the boundaries of the fault and from the use of rate-weakening friction. A comparison of simulations using scalar and vector boundary conditions for the friction on the fault suggests that slip predominantly occurs along the prestress, with the largest deviations near the rupture front and the edges of the fault.

Acknowledgments

We are grateful to Dr. S. Nielsen for useful suggestions and to Dr. Steve Day and an anonymous reviewer for comments leading to an improved manuscript. The computations in this study were partly carried out on the SGI Origin 2000 at MRL, UCSB (NSF Grant CDA96-01954), partly on the Sparc20 server at ICS, UCSB, with support from NSF Grant EAR 96-28682) and the Southern California Earthquake Center (SCEC). SCEC is funded by NSF Cooperative Agreement EAR-8920136 and USGS Cooperative Agreements 14-08-0001-A0899 and 1434-HQ-97AG01718. R. Madariaga's work was supported by Institut Universitaire de France and the Environment Program of the European Community under project SGME. This is ICS Contribution Number 0273-65EQ and SCEC Contribution Number 384.

References

Andrews, J. (1976). Rupture velocity of plane strain shear cracks, *J. Geophys. Res.* **81,** 5679–5687.

Archuleta, R. (1984). A faulting model for the 1979 Imperial Valley earthquake, *J. Geophys. Res.* **89,** 4559–4585.

Archuleta, R. and S. M. Day (1980). Dynamic rupture in a layered medium: the 1966 Parkfield earthquake, *Bull. Seism. Soc. Am.* **80,** 671–689.

Beroza, G. and T. Mikumo (1996). Short slip duration in dynamic rupture in the presence of heterogeneous fault properties, *J. Geophys. Res.* **101,** 22449–22460.

Bouchon, M. and D. Streiff (1997). Propagation of a shear crack on a

nonplanar fault: a method of calculation, *Bull. Seism. Soc. Am.* **87,** 61–66.

Brune, J. (1970). Tectonic stress and the spectra of seismic shear waves from earthquakes, *J. Geophys. Res.* **75,** 4997–5009.

Burridge, R. and J. Willis (1969). The self-similar problem of the expanding elliptical crack in an anisotropic solid, *Proc. Cambridge Phil. Soc.* **66,** 443–468.

Carlson, J. and J. Langer (1989). Mechanical model of an earthquake fault, *Phys. Rev. A* **40,** 6470–6484.

Cochard, A. and R. Madariaga (1994). Dynamic faulting under rate-dependent friction, *Pageoph* **142,** 419–445.

Cohee, B. and G. Beroza (1994). Slip distribution of the 1992 Landers earthquake and its implications for earthquake source mechanics, *Bull. Seism. Soc. Am.* **84,** 692–712.

Cotton, F. and M. Campillo (1995). Frequency domain inversion of strong motions: application to the 1992 Landers earthquake, *J. Geophys. Res.* **100,** 3961–3975.

Das, S. (1981). Three-dimensional spontaneous rupture propagation and implications for the earthquake source mechanism, *Geophys. J. R. Astr. Soc.* **67,** 375–393.

Das, S. and K. Aki (1977). A numerical study of two-dimensional spontaneous rupture propagation, *Geophys. J. R. Astr. Soc.* **50,** 643–668.

Das, S. and D. Kostrov (1983). Breaking of a single asperity: Rupture process and seismic radiation, *J. Geophys. Res.* **88,** 4277–4288.

Day, S. (1982a). Three-dimensional finite difference simulation of fault dynamics: rectangular faults with fixed rupture velocity, *Bull. Seism. Soc. Am.* **72,** 705–727.

Day, S. (1982b). Three-dimensional simulation of spontaneous rupture: the effect of nonuniform prestress, *Bull. Seism. Soc. Am.* **72,** 1881–1902.

Dieterich, J. (1978). Time-dependent friction and the mechanics of stick-slip, *Pageoph* **116,** 790–806.

Dieterich, J. (1979). Modeling of rock friction. 1. Experimental results and constitutive equations. *J. Geophys. Res.* **84,** 2161–2168.

Fukuyama, E. and R. Madariaga (1995). Integral equation method for plane crack with arbitrary shape in 3D elastic medium, *Bull. Seism. Soc. Am.* **85,** 614–628.

Fukuyama, E. and R. Madariaga (1998). Rupture dynamics of a planar fault in a 3D elastic medium: rate- and slip-weakening friction, *Bull. Seism. Soc. Am.* **88,** 1–17.

Geubelle, P. and J. Rice (1995). A spectral method for 3D elastodynamic fracture problems, *J. Mech. Phys. Solids* **43,** 1791–1803.

Harris, R. and S. Day (1993). Dynamics of fault interaction: parallel strike-slip faults. *J. Geophys. Res.* **98,** 4461–4472.

Heaton, T. (1990). Evidence for and implications of self-healing pulses of slip in earthquake rupture, *Phys. Earth Planet. Interiors* **64,** 1–20.

Ida, Y. (1972). Cohesive force across the tip of a longitudinal-shear crack and Griffith's specific surface energy, *J. Geophys. Res.* **77,** 3796–3805.

Ide, S. and M. Takeo (1997). Determination of constitutive relations of fault slip based on seismic wave analysis, *J. Geophys. Res.* **102,** 27379–27391.

Kosloff, D., D. Kessler, A. Q. Filho, E. Tessmer, A. Behle, and R. Strahilevitz (1990). Solution of the equations of dynamic elasticity by a Chebyshev spectral method, *Geophysics* **55,** 734–748.

Kostrov, B. (1964). Self-similar problems of propagation of shear cracks, *J. Appl. Math. Mech.* **28,** 1077–1087.

Kostrov, B. and S. Das (1989). *Principles of Earthquake Source Mechanics,* Cambridge U Press, New York.

Langer, J., J. Carlson, C. Myers, and B. Shaw (1996). Slip complexity in dynamic models of earthquake faults, *Proc. Natl. Acad. Sci. USA* **93,** 3825–3829.

Levander, A. (1988). Fourth-order finite-difference P-SV seismograms, *Geophysics* **53,** 1425–1436.

Madariaga, R. (1976). Dynamics of an expanding circular fault, *Bull. Seism. Soc. Am.* **66,** 639–667.

Madariaga, R. and A. Cochard (1996). Dynamic friction and the origin of the complexity of earthquake sources, *Proc. Natl. Acad. Sci. USA* **93,** 3819–3824.

Mikumo, T. and T. Miyatake (1995). Heterogeneous distribution of dynamic stress drop and relative fault strength recovered from the results of waveform inversion, *Bull. Seism. Soc. Am.* **85,** 178–193.

Miyatake, T. (1992). Reconstruction of dynamic rupture process of an earthquake with constraints of kinematic parameters, *Geophys. Res. Lett.* **19,** 349–352.

Ohminato, T. and B. A. Chouet (1997). A free-surface boundary condition for including 3D topography in the finite-difference method, *Bull. Seism. Soc. Am.* **87,** 494–515.

Ohnaka, M. (1996). Nonuniformity of the constitutive law parameters for shear rupture and quasistatic nucleation to dynamic rupture: a physical model of earthquake generation processes, *Proc. Natl. Acad. Sci. USA* **93,** 3795–3802.

Ohnaka, M. and Y. Kuwahara (1990). Characteristic features of local breakdown near crack-tip in the transition zone from nucleation to dynamic rupture during stick-slip shear failure, *Tectonophysics* **175,** 197–220.

Olsen, K. (1994). Simulation of three-dimensional wave propagation in the Salt Lake Basin. *Ph.D. Thesis,* University of Utah, Salt Lake City, Utah, 157 pp.

Olsen, K. and R. Archuleta (1996). Three-dimensional simulation of earthquakes on the Los Angeles fault system, *Bull. Seism. Soc. Am.* **86,** 575–596.

Olsen, K., R. Archuleta, and J. Matarese (1995). Three-dimensional simulation of a magnitude 7.75 earthquake on the San Andreas fault, *Science* **270,** 1628–1632.

Olsen, K., R. Madariaga, and R. Archuleta (1997). Three dimensional dynamic simulation of the 1992 Landers earthquake, *Science* **278,** 834–838.

Rice, J. and Y. Ben-Zion (1996). Slip complexity in earthquake fault models, *Proc. Natl. Acad. Sci. USA* **93,** 3811–3818.

Rice, J. R. and A. L. Ruina (1983). Stability of steady frictional slipping, *Trans. ASME J. Appl. Mech.* **50,** 343–349.

Ruina, A. (1983). Slip instability and state variable friction laws, *J. Geophys. Res.* **88,** 10359–10370.

Scholz, C. (1989). *The Mechanics of Earthquake and Faulting,* Cambridge U Press, New York.

Spudich, P. (1992). On the inference of absolute stress levels from seismic radiation, *Tectonophysics* **211,** 99–106.

Virieux, J. (1986). P-SV wave propagation in heterogeneous media: velocity-stress finite-difference method, *Geophysics* **51,** 889–901.

Virieux, J. and R. Madariaga (1982). Dynamic faulting studied by a finite difference method, *Bull. Seism. Soc. Am.* **72,** 345–369.

Wald, D. and T. Heaton (1994). Spatial and temporal distribution of slip for the 1992 Landers, California, earthquake, *Bull. Seism. Soc. Am.* **84,** 668–691.

Laboratoire de Géologie URA CNRS 1716.
Ecole Normale Supérieure, 24 rue Lhomond
75231 Paris Cedex 05, France
and Laboratoire de Sismologie
Université Denis Diderot de Paris 7
(R.M.)

Institute for Crustal Studies
UC Santa Barbara
Santa Barbara, California 93016-1100
(K.O., R.A.)

Manuscript received 27 August 1997.